NJC

Accepted Manuscript

This is an *Accepted Manuscript*, which has been through the Royal Society of Chemistry peer review process and has been accepted for publication.

Accepted Manuscripts are published online shortly after acceptance, before technical editing, formatting and proof reading. Using this free service, authors can make their results available to the community, in citable form, before we publish the edited article. We will replace this *Accepted Manuscript* with the edited and formatted *Advance Article* as soon as it is available.

You can find more information about *Accepted Manuscripts* in the Information for Authors.

Please note that technical editing may introduce minor changes to the text and/or graphics, which may alter content. The journal's standard Terms & Conditions and the Ethical guidelines still apply. In no event shall the Royal Society of Chemistry be held responsible for any errors or omissions in this *Accepted Manuscript* or any consequences arising from the use of any information it contains.

ROYAL SOCIETY OF CHEMISTRY

www.rsc.org/njc

Journal Name

RSCPublishing

ARTICLE

A Tough Smart Elastomeric Bio-based Hyperbranched Polyurethane Nanocomposite

Cite this: DOI: 10.1039/xoxxoooooox

Suman Thakur and Niranjan Karak*

Received ooth January 2012,
Accepted ooth January 2012

DOI: 10.1039/xoxxoooooox

www.rsc.org/

Herein, we fabricate an elastomeric nanocomposite using castor oil-based hyperbranched polyurethane (HPU) and iron oxide nanoparticles decorated reduced graphene oxide (IO/RGO) nanohybrid by an *in-situ* polymerization technique. The designed nanocomposite not only exhibits good thermal properties but also possesses excellent mechanical properties like tensile strength (24.15 MPa), tensile modulus (28.55 MPa) and toughness (110.8 MJm^{-3}). In addition, the nanocomposite demonstrates rapid and repeatable self-healing abilities under exposure of 20-30 s microwave power input (180-360 W) and by direct sunlight exposure (10^5 lux) for 5-7.5 min. It also demonstrates excellent shape recovery ability under microwave (30-60 s) as well as direct sunlight (1-2.5 min). Thus, the studied tough polymeric material has potential advanced applications.

Introduction

The smart material which response to a stimulus is gaining significant interest in the domain of material science due to their diversified potential applications. Among them, self-healing and shape memory materials are carved more attention to the material scientist. The self-healing ability is a crucial feature of biomaterials which upsurges the survivability of natural materials.[1] However, man-made materials are susceptible to failure upon encountering damage or fracture by external factors during their service period. Thus, development of self-healing materials which can repair themselves after mechanical damage is in high demand over the past decade.[2-4] A variety of methods have been developed to access such materials especially employment of self-healing polymers (SHP). In most of the approaches, micro-capsules containing healing agents are embedded in the polymeric matrix to achieve such property.[5,6] In those cases, the healing agent is released owing to the capillary effect into the cracked place to repair it. This type of SHP can heal themselves spontaneously, as and when required. But they can be healed only once at the same location due to exhaustion of the healing agent from the containers. To overcome this short-coming, material scientists designed a three-dimensional micro-vascular network with suitable healing agent as well as 'reversible polymer' which contains reversible bonds such as non-covalent or dynamic covalent bonds.[7-9] This type healing system can be used to heal the cracked site of the material, repeatedly. As healing agents are delivered to the crack site by the three-dimensional micro-vascular network, it can heal repeatedly, even at the same location. On the other hand, the reversible bonds are able to reversibly associate and dissociate during the triggering with an external stimulus such as heat or light.[10] They tend to open immediately upon damaging on exposure of a stimulus due to the presence of such weak bonds. These dynamic bonds can repair the fractured/damaged areas by driving the polymer chains to the site through diffusion and re-entanglement above the glass transition temperature. Despite their great advances, some serious problems limit their practical applicability. Both three-dimensional micro-vascular network embedded self-healing materials and reversible polymers suffer from poor mechanical properties along with high cost.[11,12]

Thus, development of a novel SHP with repeated healing efficiency and outstanding mechanical properties is still a key challenge. To address this problem, Huang and co-workers designed a polyurethane/graphene nanocomposite as a self-healing material.[13] These nanocomposites demonstrated repeated healing efficiency by infrared (IR) light, electricity and microwave (MW) energy with good mechanical property. However, to achieve such healing properties the amount of graphene as well as used MW power is quite high. Thus, use of such stimuli has difficulty in practical field applications. Thus, emerging materials having rapid and repeatable self-healing

capability with adequate mechanical properties still remain a daunting challenge.

Recently, a new concept has been explored on the use of shape memory materials such as shape memory alloy (SMA) based wires and shape memory polymer (SMP) based fibers to improve the self-healing process by providing a mechanism to repair the crack, partially or fully.[14,15] This can also offer repeated healing capability with improved mechanical properties. But it also suffers from some inadequacies. In order to achieve effective healing, SMA wires or SMP fibers have to be positioned locally and perpendicular to the crack.[16] This is indeed a challenge to achieve in practical applications. Thus, SMP without any external shape memory material has an immense potential to overcome the above mentioned shortcoming. In this context, Rowan et al. designed a semicrystalline polydisulfide network which inherently exhibited both shape-memory and healable properties.[17] This polydisulfide network demonstrated thermo shape-memory and photohealable properties. Also, Zhao and his co-workers fabricated polyethylene/carbon black nanocomposites which showed improved self-healing by a shape memory effect.[18] But these materials did not show multistimuli responsive behavior.

In the current scenario, hyperbranched polyurethanes (HPU)/reduced graphene oxide (RGO) nanocomposite exhibited multistimuli responsive shape memory behavior under MW, sunlight and thermal energy.[19] In addition, use of iron oxide/RGO (IO/RGO) nanohybrid instead of RGO only has some advantages as IO nanoparticle has good thermal conductivity, magnetic behavior and MW absorbing capacity. Also, RGO contains some functional groups on its surface so dispersion into the polymer matrix is easy.[20,21] Here, it is pertinent to mention that self-healing by a natural stimulus like sunlight is an eco-friendly, inexpensive and practical strategy and hence more promising. Ghosh and Urban developed a polyurethane based on oxetane substituted derivative of chitosan which can mend themselves under exposure of sunlight.[8] Most importantly RGO also has excellent sunlight absorbing capacity like graphene and hence it can be used for this purpose.[22] Furthermore, IO nanoparticles are well-known for its good microwave absorbing capacity, excellent thermal conductivity, high magnetic saturation value etc.[23] Therefore, IO/RGO nanohybrid can be used to enjoy their combined effects.

Herein, a tough self-healing elastomeric nanocomposite of HPU and IO/RGO nanohybrid was fabricated. Evaluations of mechanical properties, multi-stimuli self-healing and shape memory behavior of the nanocomposite by sunlight and microwave were performed.

Experimental

Materials

Castor oil (Sigma Aldrich), 1, 4-butanediol (BD, Merck, Germany) and poly(ε-caprolactone) diol (PCL, M_n= 3000 g mol^{-1}, Solvay Co., UK) were used after drying in an oven prior to use. Ferrous chloride (Merck, India), anhydrate ferric chloride (Merck, India) and 2, 4/2, 6-toluene diisocyanate (TDI, Merck, Germany) were used as received. Xylene (Merck, India) and N, N-dimethylacetamide (Merck, India) were vacuum distilled and kept it in 4A type molecular sieves before use. Other chemicals and solvents were used without further purification. Graphene oxide (GO) was prepared by modified Hummers method. Oxidization of graphite powder was achieved by using a mixture of concentrated sulphuric acid and $KMnO_4$ as reported in our earlier work.[20] Monoglyceride of the castor oil was prepared as reported earlier.[24]

Preparation of iron oxide/reduced graphene oxide (IO/RGO) nanohybrid

The nanohybrid was prepared by co-precipitation of ferrous and ferric ions on the GO sheets followed by reduction of GO as reported in our earlier work.[25] Briefly, 64.8 mg of $FeCl_3$ and 39.6 mg of $FeCl_2$ was mixed with 50 mL of GO dispersion in millipore water (1mg.mL^{-1}). Then the mixture was stirred constantly for 1 h under the N_2 atmosphere. Then 20 mL of banana peel ash extract and 10 mL of *Colocasia esculenta* leaf extract were added and stirred for 30 min to obtain RGO and IO nanoparticles based nanohybrid. The ratio of iron oxide and reduced graphene oxide in the nanohybrid is 1:1 in the prepared nanohybrid.

Preparation of hyperbranched polyurethane iron oxide/reduced graphene oxide (HPU-IO/RGO) nanocomposite

A three-neck round bottomed flask equipped with a nitrogen gas inlet, a mechanical stirrer and a Teflon septum was used for the nanocomposite preparation. Required amounts of PCL (0.002 mol), BD (0.004 mol) and dispersed IO/RGO nanohybrid (in DMAc) were taken in the round bottomed flask containing desired amount of xylene with constant stirring (37% solid content). After dissolving PCL, desired amount of TDI (0.007 mol) was added dropwise by help of a syringe into the reaction mixture at room temperature. The reaction was continued for 3 h at temperature of (70±2) ºC to obtain the desired viscous mass, which was treated as the pre-polymer.

This pre-polymer was then cooled to room temperature and monoglyceride of castor oil (0.002 mol) as a triol was added with the required amount of TDI (0.002 mol) to maintain the overall NCO/OH ratio equal to one. The temperature was then raised to (110±2) ºC and stirred continuously for 2.5 h to complete the reaction as indicated by the absence of isocyanate band at 2270 cm-1 in FTIR spectrum. Hyperbranched polyurethane was also prepared without using IO/RGO nanohybrid. Hyperbranched polyurethane nanocomposites with 0.5, 1 and 2 weight% of IO/RGO nanohybrid are encoded as HPU-IO/RGO0.5, HPU-IO/RGO1 and HPU-IO/RGO2 respectively, and hyperbranched polyurethane without IO/RGO nanohybrid is coded as HPU.

Instruments and Testing methods

The tensile strength and elongation at break were measured by the help of Universal Testing Machine (UTM), Jinan WDW 10,

Republic of China with a 500 N load cell and crosshead speed of 20 mm.min-1. The differential scanning calorimetry (DSC) study was done by using DSC 6000, Perkin Elmer, USA at heating rate of 2 oC min-1 under the nitrogen flow rate of 30 mL min-1 from -20 to 120 °C. TGA was done by thermal analyzer, TGA 4000 (Perkin Elmer, USA) with a nitrogen flow rate of 30 mLmin-1 at heating rate of 10 °C min-1.

In order to evaluate the healing performance, the films with thickness of 0.5 mm of the nanocomposite were cut (10 × 0.2 × 0.015 mm^3 in dimension) in transverse direction by a razor blade and the cracked was healed by sunlight and microwave, separately. Healing efficiency was calculated as the ratio of tensile strength values of the nanocomposites before to after healing. The tensile strengths of the pristine and the healed samples were measured by the same UTM. Samples were cut into strips of 80 × 10 × 0.50 mm^3 for testing. Tensile strengths of pristine HPU as well as nanocomposites with different loadings of nanohybrid were measured for at least 5 samples in each case, before and after healing process. The optimal healing time for each case is defined as the shortest time required to achieve the best healing efficiency under the given conditions. For MW healing, a domestic microwave oven (800 W) at operating frequency of 2.45 GHz was used. Three different MW power (180, 360 and 540W) were used for healing. Sunlight healing was performed under direct sunlight (11 am-2 pm) at Tezpur University campus (altitude: 26.63 °N 92.8 °E) in the month of November at sunny days [average temperature (29±1 °C) and humidity (65±1 %)], light intensity: 90,000-100,000 lux.

To study the shape memory behavior under MW and direct sunlight, the bending test was performed. The sample was folded in ring form at 60 °C followed by quenching into an ice-salt bath for 5 min at -10 °C. Then the shape recovery of the nanocomposite films was achieved by exposing MW irradiation of 360 W for 30-60 s under ambient condition or by direct sunlight in sunny days of November, 2013. The shape recovery was calculated using the following equation.

Shape recovery (%) = {(90-θ)/90} ×100 ---------- (1)

Where θ in degree denotes the angle between the tangential line at the midpoint of the sample and the line connecting the midpoint and the end of the curved sample.

Results and Discussion

Preparation of the nanocomposite

An *in-situ* polymerization technique was used to prepare the HPU-IO/RGO nanocomposite by using monoglyceride of castor oil as a branch generating moiety and IO/RGO as the reinforcing nanomaterial as shown in Scheme 1. It is pertinent to mention here that the average functionality of castor oil is about 2.7, but the monoglyceride of it contains little amount of unreacted glycerol, castor oil and diglyceride. Thus, average functionality of monoglyceride is considered 3 for simplicity.

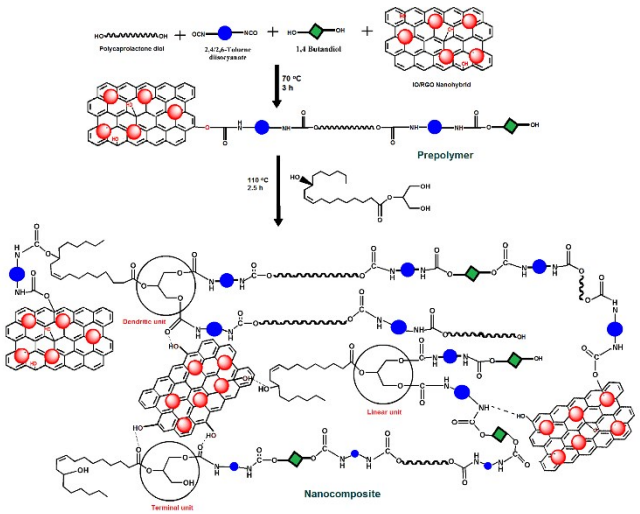

Scheme 1 Synthesis of HPU-IO/RGO nanocomposite.

The crucial monitoring factors during nanocomposite preparation are concentration of the reactants (especially multifunctional moiety), addition rate of the multifunctional moiety, reaction time and temperature.[26] During the nanocomposite preparation, dispersion of IO/RGO nanohybrid in DMAc was incorporated in the 1st step of polymerization to obtain strong interfacial interaction of it (covalent and noncovalent) with HPU chains. In the 2nd step of the reaction, multifunctional moiety was slowly added in a very dilute solution (15% in xylene) to avoid gel formation and also temperature of the reaction was gradually raised to 110 °C.[26]

Characterization of nanocomposite

FTIR spectra are confirmed the presence of urethane linkage both in HPU and its nanocomposites (Fig. 1). In the studied HPU and its nanocomposites, the appeared vibration bands at 1680-1695 cm^{-1} were attributed to C=O stretching vibration (contribution from both amide I and ester linkage). Further, N-H stretching and N-H bending vibrations were observed at 3430 and 1557–1580 cm^{-1} respectively. A few more characteristic bands for urethane linkage were found at 1060-1090 cm^{-1} (N-H deformation vibration), 1140-1175 cm^{-1} (C-O stretching vibration) etc.[24,26] The shifting of C=O band to 1680 from 1695 cm^{-1} was observed with the increasing amount of IO/RGO in the nanocomposite.[26] This indicates the presence of interactions among polymer chains and IO/RGO nanohybrid. These interactions increase with the increase of IO/RGO content.

In XRD patterns, HPU and its nanocomposite exhibited two distinct peaks at 2θ = 21.15° (corresponding to d-spacing of 0.41 nm) and 23.5° (corresponding to d-spacing of 0.375 nm) which are attributed to the crystals of PCL moiety present in HPU (Fig. 2).[26] After incorporation of nanohybrid, a slight shifting of the PCL peaks towards higher angle was observed which may be due to formation of dense structure compared to the pristine HPU.[26] Also the peak intensity of PCL moiety was little increased with loading of nanohybrid.

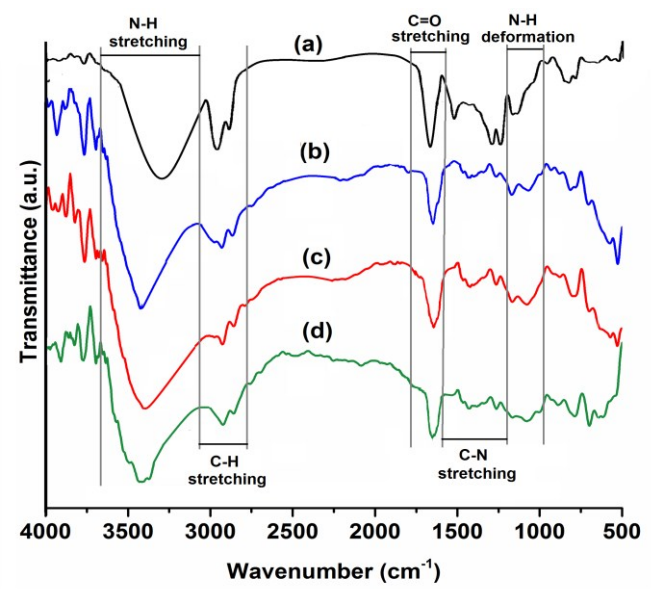

Fig. 1 FTIR spectra of (a) HPU, (b) HPU-IO/RGO0.5, (c) HPU-IO/RGO1 and (d) HPUIO/RGO2.

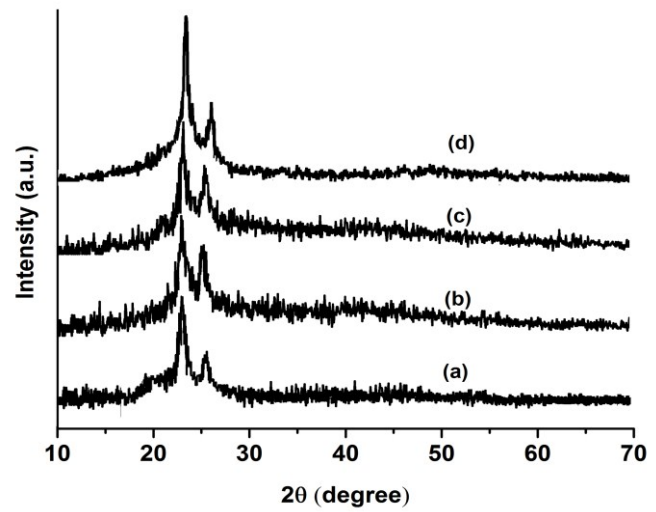

Fig. 2 XRD patterns of (a) HPU, (b) HPU-IO/RGO0.5, (c) HPU-IO/RGO1 and (d) HPU-IO/RGO2.

This indicates that the crystallinity of the nanocomposite increased with increase dose of nanohybrid as nanohybrid acts as a nucleating agent. Here it is pertinent to mention that no such distinct peak is observed for IO/RGO in the XRD patterns of nanocomposites. This may be due to the presence of a small amount of IO/RGO in the nanocomposite.

The performance of nanocomposites strongly influenced by the dispersion of nanohybrid in the HPU matrix. Therefore, HRTEM was employed to investigate the dispersion of nanohybrid. HRTEM images of HPU-IO/RGO 2 are shown in Fig. 3. From the figure, it is cleared that nanohybrid is finely distributed in the HPU matrix.

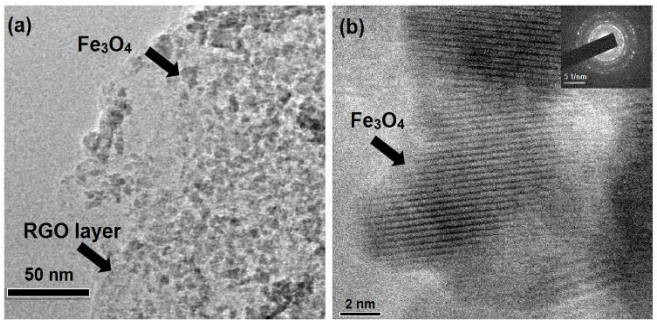

Fig. 3 HRTEM images of HPU-IO/RGO2: (a) at low resolution showing RGO layer and decorated IO nanoparticle and (b) at high resolution showing an individual IO nanoparticle on RGO sheet (inset showing SAED patterns).

Mechanical properties

The pristine HPU possesses low tensile strength and modulus due to the presence of hyperbranched structure and monoglyceride of castor oil in the polymer chains. After incorporation of IO/RGO nanohybrid, all the nanocomposites exhibited excellent dose dependent mechanical properties like tensile strength, tensile modulus and toughness (Table 1). The noticeable achievement of this study is a simultaneously improvement of tensile strength and elongation at break which resulted in high toughness for the nanocomposite. Such outstanding mechanical properties can definitely be attributed to the strong interfacial adhesion and good compatibility between HPU and the nanohybrid.[26,27] Also the remaining hydroxyl groups in the nanohybrid may react with isocyanate terminated prepolymer chain to form a urethane linkage between HPU and the nanohybrid.[21] These strong chemical bonds help to a successful transfer of the load from HPU to nanohybrid in the nanocomposite.[26] Due to the presence of the afore-stated covalent bond, H-bonding, polar-polar interaction between nanohybrid and HPU chains, the hard domain of HPU is stiffened. This consequently enhances tensile modulus of the nanocomposite. The nanocomposite also demonstrated high dose dependent toughness after incorporation of nanohybrid. These nanocomposites also exhibited excellent flexibility with very high elongation at break.

Table 1. Mechanical properties of the nanocomposites

Properties	HPU*	HPU-IO/RGO 0.5	HPU-IO/RGO 1	HPU-IO/RGO 2	HPU- RGO 2#
Tensile Strength (MPa)	7.3±0.7	17.15±1.7	21.34±2.1	24.15±2.3	28.3 ± 1.9
Tensile Modulus (MPa)	3.5±0.5	10.49±0.4	18.5±0.9	28.55±1.2	37.3 ± 3.2
Toughness (MJm^{-3})	26.30±2.8	41.8 ±5.4	66.4 ±6.1	110.8 ±5.4	121.78 ± 4.1
Elongation at break (%)	660±25	745±15	936±35	1090±50	1180 ± 34

*Reproduced with permission[24] and #Reproduced with permission.[30]

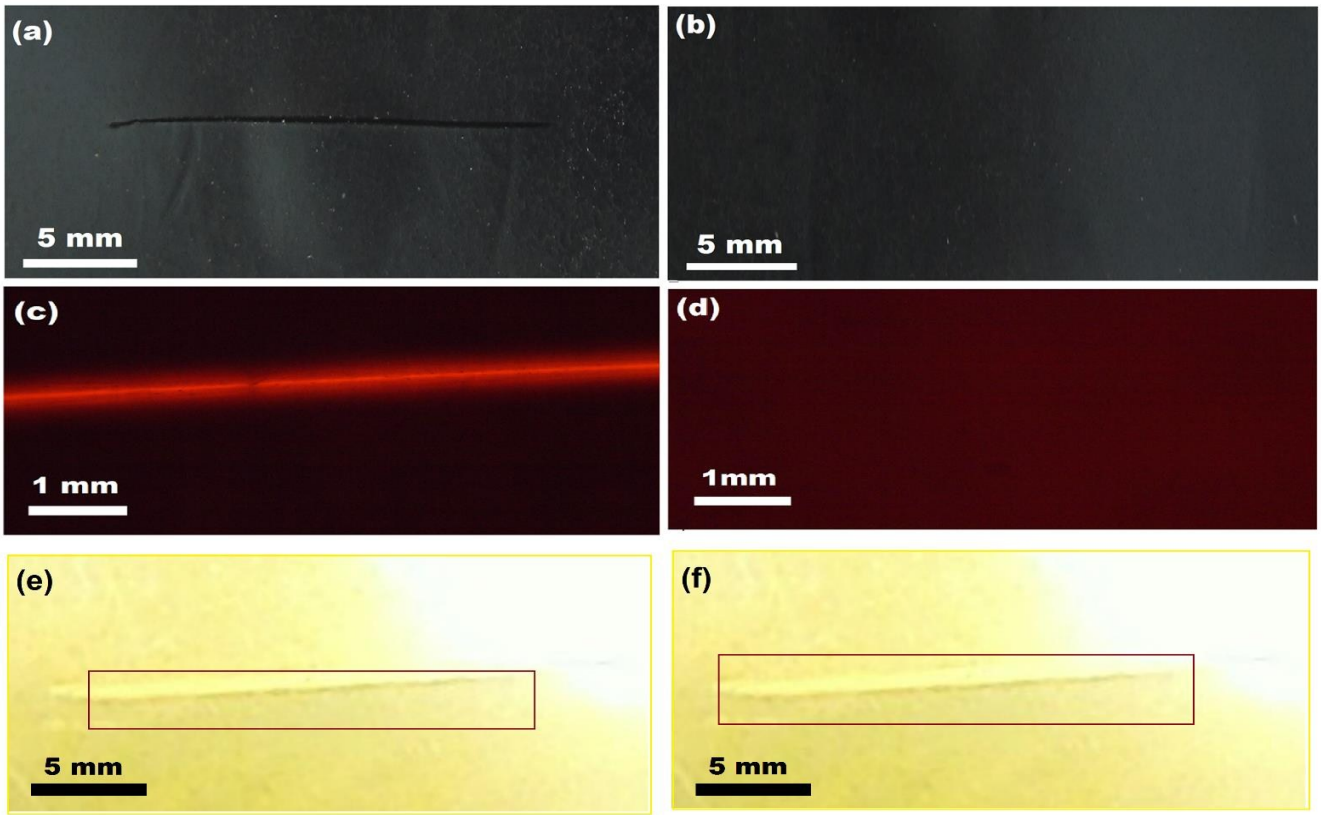

Fig. 4 Digital photographs of (a) fractured nanocomposite film and (b) healed nanocomposite film, and optical microscopic images of (c) fractured nanocomposite film and (d) healed nanocomposite film, digital photograph of HPU (e) before and (f) after healing.

More interestingly elongation at break of the nanocomposites increased with increase in content of nanohybrid. Such enhancement was noticed due to alignment of HPU chains in the initial stage of tensile loading which forces to orient the nanohybrid along the loading direction. This was also observed in other reported graphene-based polymer nanocomposites.[28,29] Again, at high stress the layer of RGO in the nanohybrid may slide each other.[30] From Table 1, a slight deterioration of mechanical properties of the HPU-IO/RGO nanocomposite is observed from the HPU-RGO nanocomposite. This may be due to presence of high aspect ratio of nanomaterial, especially RGO that provided mechanically strong nanocomposite.[30] On the other hand, only IO based HPU nanocomposite exhibited inferior mechanical properties compared to HPU-RGO nanocomposite.[31] Therefore, equal amount of RGO and IO nanoparticle containing nanohybrid was used to fabricate the nanocomposite in this investigation.

Self-healing behavior of the nanocomposite

Optical images were used to examine the healing ability of the nanocomposites. Typical optical images for the flaw film before and after healing are shown in Fig. 4. Comparison of the two optical images before and after healing clearly demonstrates the completion of the healing process of the nanocomposite film. All the nanocomposites were healed rapidly with excellent healing ability after incorporation of a small amount (0.5-2 weight %) of IO/RGO nanohybrid. On the contrary, the pristine HPU film does not heal or only partially healed even after long time exposure of any tested stimulus. The incorporation of the nanohybrid remarkably enhanced the healing abilities of HPU is clearly reflected by this result. The intrinsic properties of IO/RGO such as excellent MW absorbing capacity and high thermal conductivity, as mentioned earlier, are responsible for this observation.[21]

The healing efficiencies of the nanocomposite films under MW are shown in Fig. 5. This depicted that the nanocomposite films were healed with high healing efficiency of 99% or more. Healing efficiency of nanocomposite by MW depends on the amount of nanomaterial, power input of MW and exposure time (Fig. 5a-c). Increase in any of these parameters resulted in improvement of healing efficiency. Here, it is pertinent to mention that pristine HPU only slightly healed (10-15%) after 5 min of MW exposure. Although HPU-RGO 2 nanocomposite is completely healed within 4 min at high MW power input of 540W. Healing of HPU/IO-RGO nanocomposites is faster due to the presence of high amount of iron oxide in the nanohybrid (equal amount to RGO) which have high MW absorption capacity.[21] Therefore, the nanohybrid absorbs sufficient energy to heal the cracked rapidly.

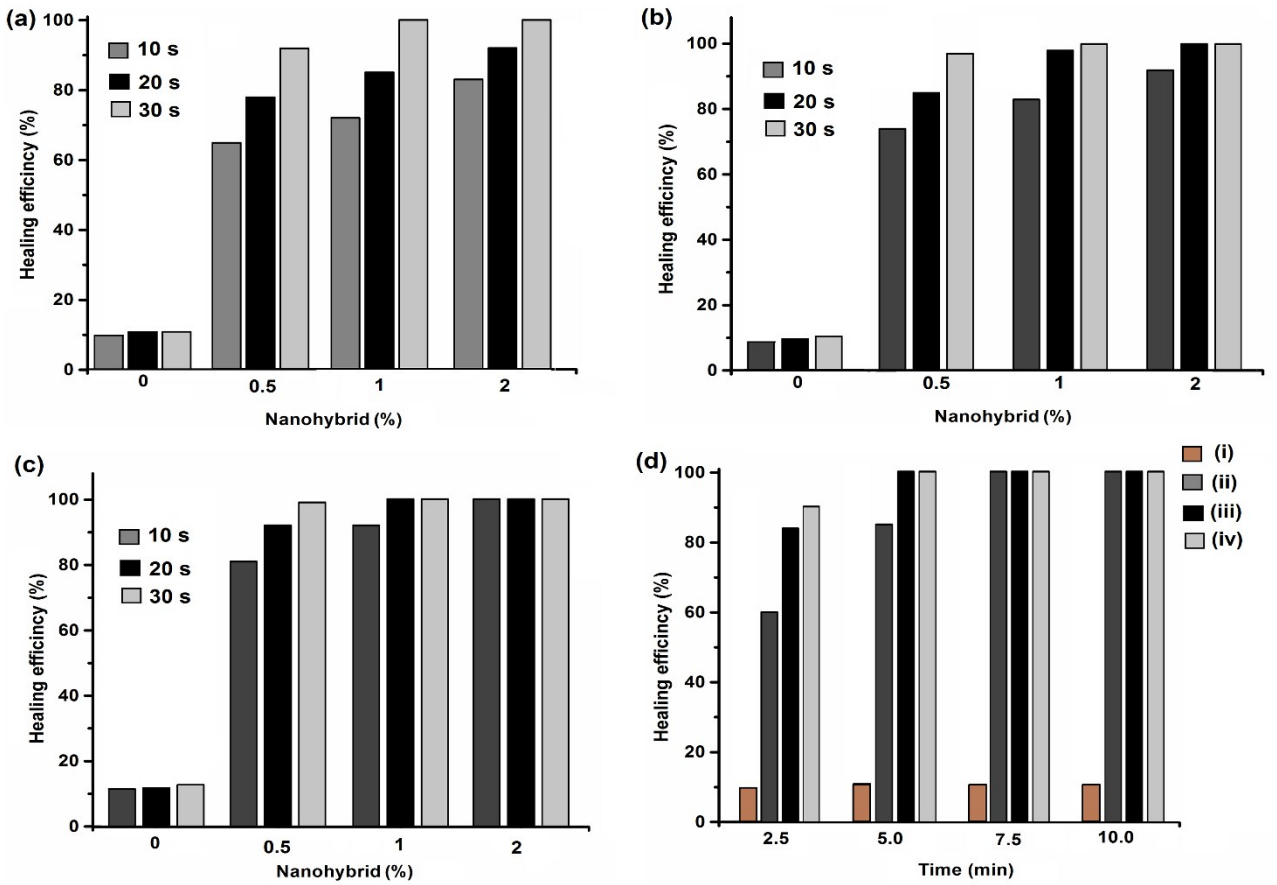

Fig. 5 The healing efficiency at MW power of (a) 180 W, (b) 360 W and (c) 540 W, and (d) under direct sunlight for different loadings of nanohybrid (i) 0%, (ii) 0.5%, (iii) 1% and (iv) 2%.

All the nanocomposites were rapidly healed within 20-30 s under low MW power (360W only). During the healing process, the nanohybrid is working as a nanoscale heater as well as heat carrier unit. The nanohybrid absorbed MW energy and started to oscillate its dipoles, the friction of which generated heat at the nanohybrid–polymer interface.[31] The energy is efficiently transferred to the HPU matrix by the nanohybrid which aids to rapid Brownian movements of the soft segment of the nanocomposite as above the transition temperature (melting temperature of the soft segment of HPU (Fig. 6). These Brownian movements of the HPU chains increases with nanohybrid loading. Hence, the nanocomposite films were heated uniformly and rapidly upon exposure to a stimulus. This helps to permanently repair the flaw as diffusion occurs at that flaw site and the process can be repeated for multiple times. HPU-IO/RGO 2 nanocomposite demonstrate faster healing compared to other studied nanocomposites although it has more molecular restriction. This is due to the presence of more amount of nanohybrid in it which helps to absorb more MW energy and helps to transfer this energy to HPU matrix for rapid healing. As self-healing was achieved by the rearrangement and diffusion of soft segments of HPU, so the healing of the prepared nanocomposite could be repeated again and again.[32] As a result, even after fifth cycle of experiment, the healing ability of the nanocomposite remains almost same (Fig. 7).

The nanocomposite with 1 and 2% of nanohybrid demonstrated rapid healing within 5 min with excellent healing efficiency under direct sunlight exposure (Fig. 5d). But the nanocomposite with 0.5% IO/RGO can only be healed after 7.5 min. These results indicate dose dependent healing as well as these loading of nanohybrid is sufficient for the healing process under sunlight. Similar to MW, the light energy is efficiently transferred throughout the nanocomposite and aids to rapid Brownian movement of molecular chains of the segment. This causes rapid healing of nanocomposite as diffusion of chains at flaw site takes place easily. Here also the nanocomposite was repeatedly healed by sunlight and even after fifth cycle of experiment no significant decrease in efficiency was observed (Fig. 7).

The study also revealed that the used energy of the stimulus is inadequate to cause any degradation or dimensional stability as confirmed by the thermal study of the nanocomposites.

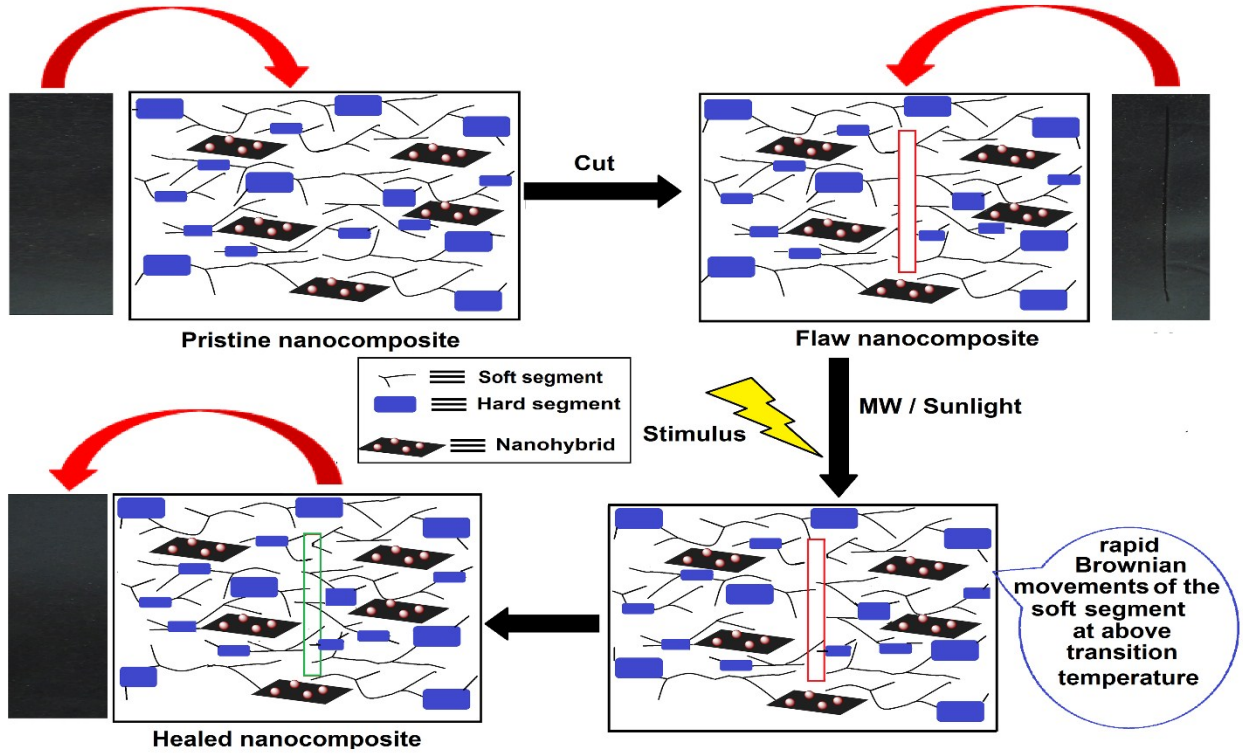

Fig. 6 Plausible healing mechanism of the nanocomposite.

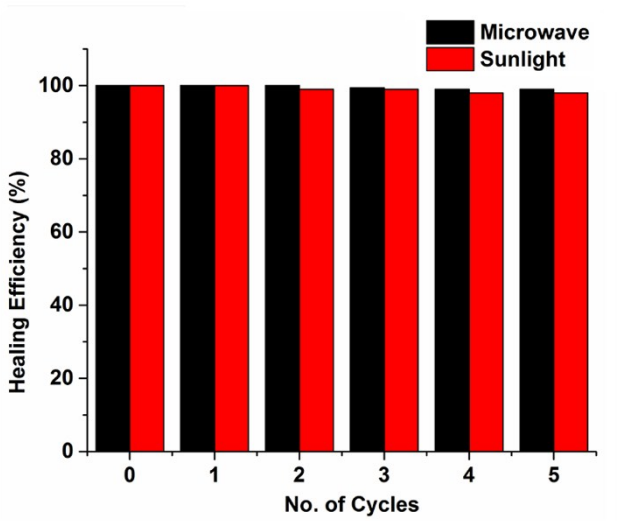

Fig. 7 Healing efficiency of HPU-IO/RGO2 nanocomposite for repeated cycles under MW (at 360 W) and sunlight stimuli.

Thermal properties

Fig. 8a demonstrated that the melting point (T_m) of soft segment (PCL moiety) is increasing from 48.2 °C to 52.4 °C upon incorporation of 2 wt% nanohybrid in HPU matrix. The presence of nanohybrid may restrict the molecular motion of the polymeric chains at initial stage.[26] This may be the reason of increment of T_m. Also, this influence depends on the interaction of the nanohybrid with the HPU chains. This clearly suggests that IO-RGO acts as a nucleating agent in the matrix and thus the presence of the nanohybrid can improve the crystallization process by bringing the arrangement of the HPU chains in a particular way.[33]

Thermogravimetric analysis (TGA) was performed to verify the thermal stability of the HPU and its nanocomposite (Fig. 8b). All the thermograms showed two steps degradation patterns. The degradation temperatures of the nanocomposites were enhanced compared to HPU. It suggests the good dispersibility of IO/RGO in the HPU matrix. The improved thermo-stability of the nanocomposites with loading of the nanohybrid is owing to limited motion of HPU chains due to the presence of different physico-chemical interactions.[34] The produced volatiles during the decomposition were also retained for a longer time in the matrix due to better barrier characteristic compared to the pristine HPU.[35]

Shape memory behavior of the nanocomposite

Furthermore, all the nanocomposites exhibited multi-stimuli responsive shape memory behaviors. Shape memory behaviors of the nanocomposite by MW were shown in Fig. 9. Shape memory tests were also performed under the exposure of MW and sunlight. Shape recovery time and ratio under different stimuli are tabulated in Table 2. In all cases, the shape recovery time decreased with the increase of nanohybrid content in the nanocomposites.

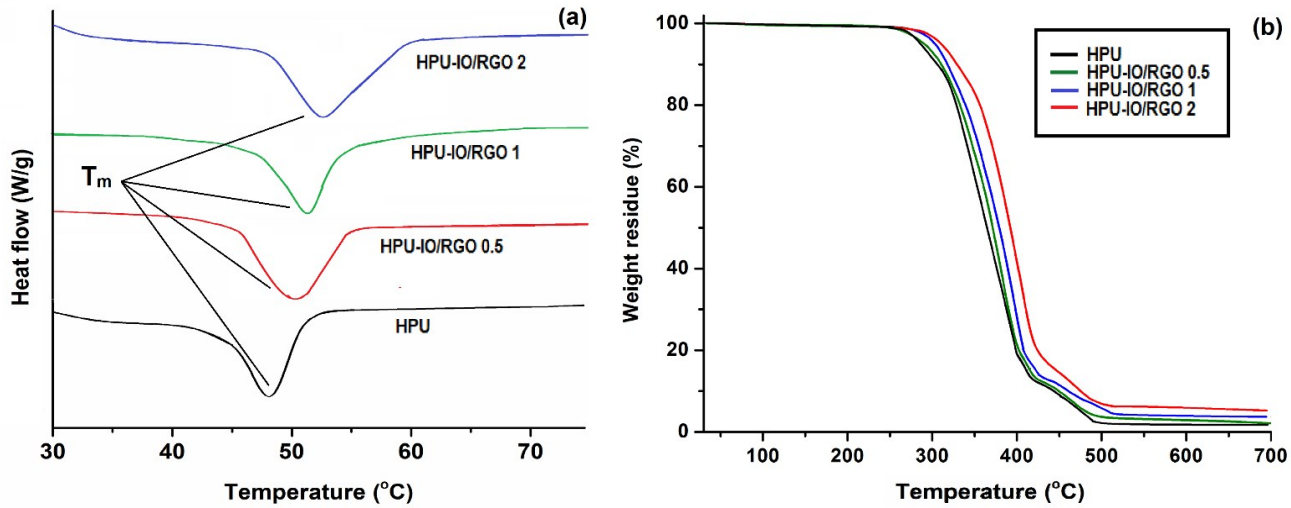

Fig. 8 a) DSC curve showing melting temperature of soft segment of HPU and its nanocomposites and (b) TGA themrograms of HPU and its nanocomposites.

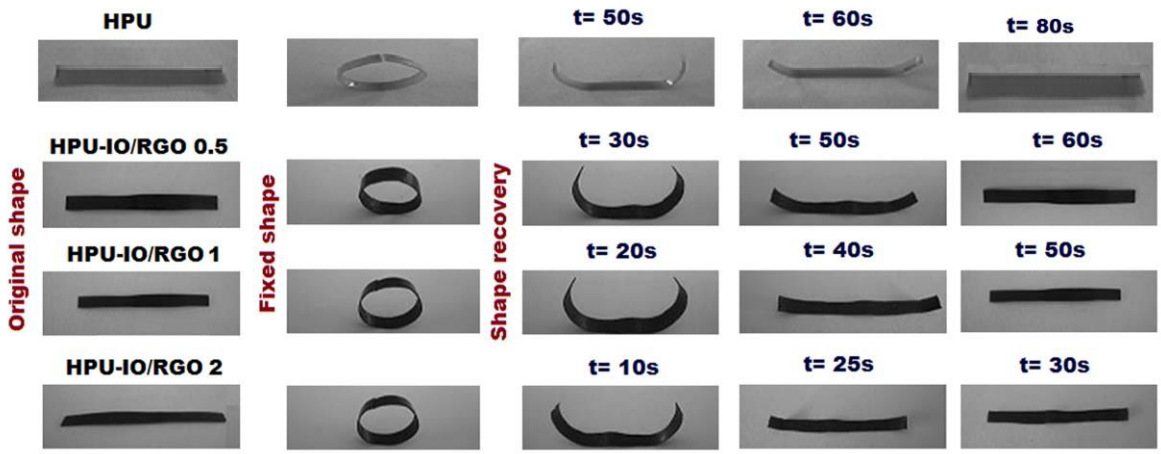

Fig. 9 Shape memory behavior of the nanocomposites under MW stimulus.

Table 2. Shape memory properties of the nanocomposites

Stimulus		HPU	HPU-IO/RGO 0.5	HPU-IO/RGO 1	HPU-IO/RGO 2	HPU-RGO 2
MW	Shape recovery time (s)	80	60	50	30	53
	Shape recovery (%)	95.5	96.4	97.4	99	97.6
Sunlight	Shape recovery time (min)	7	2.5	2	1	1.5
	Shape recovery (%)	95.3	96.1	97.2	98.5	98.1

Nanohybrid created a large amount of stored elastic strain energy due to strong interfacial interactions with the compatible HPU matrix.[26] This assisted the nanocomposites to achieve a high recovery speed due to the release of stored elastic strain. Also, enhancement of MW and sunlight absorbing capacity with the increase of the nanohybrid content is another important factor for fast recovery.

Conclusions

In summary, we demonstrated a self-healable and shape recoverable hyperbranched polyurethane nanocomposite with outstanding mechanical properties. The obtained nanocomposites exhibited repeatable and rapid healing ability by different stimuli namely microwave and sunlight as well as excellent shape memory behavior under the same stimuli. In contrast to the existing reported self-healing systems, these nanocomposites showed rapid and repeatable healing ability under green stimuli especially sunlight which is eco-friendly, inexpensive and practically useful. A few more stimuli such as magnetic, electric and infrared light may also be used for the same purpose. The nanocomposite has potential applications in transport, construction, electronics and so forth industries.

Acknowledgements

S.T. sincerely acknowledges the receipt of his Senior Research Fellowship from the Council of Scientific and Industrial

Research (CSIR), India. The authors also express their gratitude to FIST program-2009 (DST), India through the grant No.SR/FST/CSI-203/209/1 dated 06.05.2010. The research is funded by Department of Science and Technology (DST), India through the grant No. SR/S3/ME/0020/2009-SERC, dated 9th July, 2010.

Notes and references

Advanced Polymer and Nanomaterial Laboratory, Centre for Polymer Science and Technology, Department of Chemical Sciences, Tezpur University, Tezpur 784028, India.
Fax: +91 3712-267006; Tel: +91 3712-267327;
E-mail: karakniranjan@gmail.com (N. Karak)

1 R. J. Varley, D. A. Craze, A. P. Mouritz and C. H. Wang, *Macromol. Mater. Eng.* 2013, **298**, 1232–1242.
2 R. P. Wool, *Soft Matter*. 2008, **4**, 400–418.
3 B. C. Tee, C. Wang, R. Allen and Z. Bao, *Nat. Nanotechnol.* 2012, **7**, 825 – 832.
4 H. P. Cong, P. Wang and S. H. Yu, *Chem. Mater*. 2013, **25**, 3357-3362.
5 E. Koh, S-Y. Baek, N-K. Kim, S. Lee, J. Shin and Y.-W. Kim, *New J. Chem*. 2014, **38**, 4409-4419.
6 S. R. White, N. R. Sottos, P. H. Geubelle, J. S. Moore, M. R. Kessler, S. R. Sriram, E. N. Brown and S. Viswanathan, *Nature* 2001, **409**, 794-797.
7 X. X. Chen, M. A. Dam, K. Ono, A. Mal, H. B. Shen, S. R. Nutt, K. Sheran and F. Wudl, *Science* 2002, **295**, 1698−1702.
8 B. Ghosh and M. W. Urban, *Science* 2009, **323**, 1458−1460.
9 Y. Amamoto, J. Kamada, H. Otsuka, A. Takahara and K. Matyjaszewsk, *Angew. Chem. Int. Ed.* 2011, **50**, 1660–1663.
10 M. Burnworth, L. Tang, J. R. Kumpfer, A. J. Duncan, F. L. Beyer, G. L. Fiore, S. J. Rowan and C. Weder, *Nature* 2011, **472**, 334−337.
11 R. S. Trask and I. P. Bond, *Smart Mater. Struct.* 2006, **15**, 704−710.
12 D. Y. Wu, S. Meure and D. Solomon, *Prog, Polym. Sci.* 2008, **33**, 479−522.
13 L. Huang, N. Yi, Y. Wu, Y. Zhang, Q. Zhang, Y. Huang, Y. Ma and Y. Chen, *Adv. Mater*. 2013, **25**, 2224–2228.
14 S. Neuser, V. Michaud and S. R. White, *Polymer* 2012, **53**, 370–378.
15 G. Li, H. Meng and J. Hu, *J. R. Soc. Interface* 2012, **9**, 3279– 87.
16 X. Luo and P. T. Mather, *ACS Macro Lett*. 2013, **2** *(2)*, 152–156.
17 B. T. Michal, C. A. Jaye, E. J. Spencer, S. J. Rowan, *ACS Macro Lett.* 2013, **2**, 694–699.
18 X. Wang, J. Zhao, M. Chen, L. Ma, X. Zhao, Z. Dang, Z. Wang, *J. Phys. Chem. B* 2013, **117**, 1467– 1474.
19 S. Thakur and N. Karak, *J. Mater. Chem. A*, 2014, **2**, 14867–14875.
20 S. Thakur and N. Karak, *Carbon* 2012, **50**, 5331-5339.
21 X. Zhao, Z. Zhang, L. Wang, K. Xi, Q. Cao, D. Wang, Y. Yang and Y. Du, Sci Rep 2013; 3: DOI: 10.1038/srep03421.
22 M. Bernardi, M. Palummo and J. C. Grossman, *Nano Lett.* 2013, **13**, 3664−3670.
23 Y. J. Chen, P. Gao, C. L. Zhu, R. X. Wang, L. J. Wang, M. S. Cao and X. Y. Fang, *J. Appl. Phys.* 2009, **106**, 054303.
24 S. Thakur and N. Karak, *Prog. Org. Coat*. 2013, **76**, 157–164.
25 S. Thakur and N. Karak, *Mater. Chem. Phys.* 2014, **144**, 425-432.
26 S. Thakur and N. Karak, *RSC Adv.* 2013, **3**, 9476-9482.
27 D. Cai, J. Jin, K. Yusoh, R. Rafiq and M. Song, *Compos. Sci. Technol.* 2012, **6**, 702–707.
28 J. R. Potts, D. R. Dreyer, C. W. Bielawski and R. S. Ruoff, *Polymer* 2011, **52**, 5-25.
29 X. Wang, Y. Hu, L. Song, H. Yang, W. Xing and H. Lu, *J. Mater. Chem.* 2011, **21**, 4222-4427.
30 S. Thakur and N. Karak, *ACS Sustainable Chem. Eng.* 2014, **2**, 1195–1202.
31 H. Kalita and N. Karak, *Polym. Bull*. 2013, **70**(11), 2953-2965.
32 Y. Bai, Y. Chen, Q. Wang and T. Wang, *J. Mater. Chem. A* 2014, **2**, 9169-9177.
33 R. M. Hodlur and M. K. Rabinal, *Compos. Sci. Technol.* 2014, **90**, 160-165.
34 R. K. Layek, A. Kundu, A. K. Nandi, *Macromol. Mater. Eng.* **2013**, *298*, 1166–1175.
35 F. H. Jeong, J. Yang, H. S. Lee, S. W. Seo, D. H. Baik and J. Kim, *J. Appl. Polym. Sci.* **2008**, *107*, 803-809.